CARBON 59 (2013) 487–494

Available at www.sciencedirect.com

SciVerse ScienceDirect

journal homepage: www.elsevier.com/locate/carbon

Raman spectroscopy of morphology-controlled deposition of Au on graphene

Caiyu Qiu [a], Haiqing Zhou [a,b], Bingchen Cao [a], Lianfeng Sun [d], Ting Yu [a,c,*]

[a] Division of Physics and Applied Physics, School of Physical and Mathematical Sciences, Nanyang Technological University, Singapore 637371, Singapore

[b] Department of Chemistry, Rice University, 6100 Main Street, Houston, TX 77005, United States

[c] Department of Physics, Faculty of Science, National University of Singapore, Singapore 117542, Singapore

[d] National Centre for Nanoscience and Technology, Beijing 100190, China

ARTICLE INFO

Article history:
Received 23 December 2012
Accepted 23 March 2013
Available online 3 April 2013

ABSTRACT

By tuning substrate temperatures in a thermal deposition process, Au nanostructures with different morphologies, such as polygons, dendrites, irregular islands and dense clusters have been obtained on graphene surface. The surface-enhanced Raman scattering (SERS) of graphene caused by gold decoration is systematically investigated. The enhancement factor of graphene G band and the extent of G band splitting are found to be dependent on the morphologies of gold clusters. A maximum enhancement factor as high as ~270 is obtained for polygonal gold film deposited on monolayer graphene. Furthermore, as a SERS substrate, graphene combined with polygonal gold shows the highest Raman enhancing efficiency for crystal violet (CV) molecules. The mechanisms for the above results are discussed.

1. Introduction

Raman spectroscopy is widely used as a nondestructive technique to probe the characteristics of graphene. By analyzing the features of the characteristic G-, D-, and 2D (or G′)-Raman modes, we can obtain considerable information about graphene, such as the layer number [1,2], stacking order [3,4], the electronic structure [5,6], edge structure [7,8], dopants [9,10] and strain-induced mechanical deformation [11,12]. The well-established Raman investigations of graphene make it an ideal system for detailed study of surface-enhanced Raman scattering (SERS) effects. Meanwhile, SERS can enhance Raman signals by several orders of magnitude, and thus facilitate the ultrasensitive detection of subtle properties of graphene and other molecules.

Conventional SERS-active systems, such as rough metallic surfaces, colloidal metal nanoparticles, metal islands, and fractal films, are mainly based on the laser induced surface plasmon resonance (SPR) supported by nanostructured conducting materials [13]. The SPR-mediated enhancement of electric field will amplify the Raman cross section of molecules adsorbed on plasmonic nanostructures. This enhancement mechanism is called electromagnetic mechanism (EM). Several parameters, including the structure, shape, size, density and metal species, greatly affect the SPR behavior and ultimately influence the SERS properties [14,15]. In addition, it is generally accepted that the second and less prominent mechanism contributing to the SERS phenomenon is chemical mechanism (CM), which results from an increased molecular polarizability [16].

The enhancement of Raman signal from mechanically exfoliated graphene has been obtained through different approaches. The commonly used SiO_2/Si substrate has been found to enhance the Raman signal of graphene by ~30 times

* *Corresponding author at:* Division of Physics and Applied Physics, School of Physical and Mathematical Sciences, Nanyang Technological University, Singapore 637371, Singapore. Fax: +65 63167899.
E-mail address: yuting@ntu.edu.sg (T. Yu).

0008-6223/$ - see front matter © 2013 Elsevier Ltd. All rights reserved.
http://dx.doi.org/10.1016/j.carbon.2013.03.043

due to the so called interference-enhanced Raman scattering (IERS) in the SiO_2 layer [17]. Utilizing Si substrates capped with designed metal and metal oxide double layers, the Raman intensity of graphene can be enhanced greatly through a combination of IERS and SERS [18]. Recently, some studies have investigated the SERS of graphene through the metal deposited on it. For instance, an enhancement factor (EF) of 60, under 633 nm excitation, has been reached for single-layer graphene covered with well-defined gold disc arrays [19]. Lee et al. have increased the EF to 120 by substituting thermally deposited gold nanoparticles for gold disc arrays [20]. They also investigated SERS of graphene covered by Ag, and the average SERS enhancement factor of the G band for monolayer graphene is around 24 [21]. More experiments exploring new plasmonic nanostructures for SERS of graphene are helpful to further understand the SERS phenomena and important for the research on graphene.

In this work, gold is chosen for its stability and resistance to corrosion. Au films of 4 nm are thermally deposited with different morphologies on graphene/SiO_2 (300 nm)/Si system. After that, SERS spectra of gold-decorated monolayer graphene are measured. The EFs of the G and 2D peaks show different dependence on the detailed morphologies of gold films. In particular, a maximum EF of ~270 of G band can be obtained from the gold film with polygonal structure at 633 nm excitation. By analyzing the G band splitting in the SERS spectra, the mechanical modification of graphene given by these gold films is qualitatively exploited. Furthermore, Raman signals of crystal violet (CV) molecules adsorbed on these gold-decorated graphenes which are used as SERS substrates are compared. The results further confirm that the highest enhancement efficiency is given by the gold film consisting polygonal particles.

2. Experimental details

Graphene samples were prepared onto a silicon wafer with an insulating SiO_2 layer of 300 nm by micromechanical cleavage of natural graphite flakes (Alfa Aesar). The layer number of graphene was initially distinguished according to the color contrast under an optical microscope (OM, Leica DM4000), and was further identified by micro-Raman spectroscopy (Renishaw inVia Raman Spectroscope) [22].

Recent work has elucidated that the optimized experimental conditions for gold induced SERS of graphene are: Au layers of 4 or 5 nm in thick under 633 nm laser excitation [20]. Based on this finding, a 4 nm thick layer of gold was thermally deposited onto graphenes. The deposition of gold was performed by resistively heating a ceramic crucible under a vacuum of $\sim 10^{-4}$ Pa with a rate of 1.0 Å/s. Final thickness (4 nm) was monitored by a quartz crystal microbalance in the evaporator chamber [23]. In order to acquire different morphologies of gold, the substrate temperature was elevated to certain values in a controlled manner during gold deposition. In detail, the wafer with graphene samples was attached onto a power film resistor (Caddock MP9100) which is parallel to the horizontal crucible. By running a set current through the resistor, the temperature of the SiO_2/Si substrate can be monitored from room temperature to 160 °C. To examine the morphologies of gold nanostructures on graphenes, scanning electron microscopy (SEM, Hitachi S-4800) was used at an accelerating voltage of 5 kV.

To test the different SERS effects on various substrates, CV dye molecules were deposited by immersing samples in CV solution with concentration of 2×10^{-6} M. The soaking time was 2 h, so that the adsorption equilibrium was reached. Then the samples were rinsed with deionized water (DI) and dried gently using N_2 flow.

For SERS studies, the micro-Raman experiments were performed under ambient conditions using 633 nm (1.96 eV) He–Ne excitation source. To diminish laser induced heating, the laser power was kept at ~ca. 1.0 mW. For precision, a 100× objective lens with a numerical aperture of 0.90 was used leading to a ~1 μm laser spot size. Meanwhile, a 250 mm focal length spectrograph and a high-resolution 1800 grooves/mm grating make a spectral resolution of ~2 cm^{-1}. Before each data acquisition, the intensity of the Raman peak at 520 cm^{-1} from silicon was normalized. Every spectrum was taken with a total accumulation time of 20 s and other parameters were also set to be identical.

3. Results and discussion

3.1. Gold deposition and SEM characterization

By means of keeping the substrate at controlled temperatures, after 4 nm gold film deposition on graphenes, four different Au morphologies were obtained. The corresponding SEM images are displayed in Fig. 1(a)–(d). According to their characteristics, we name these gold nanostructures by letters P (polygons), D (dendrites), I (irregular islands) and C (dense clusters). Here, the gold film "C" shown in Fig. 1(d) was deposited at room temperature [20,24]. The other three gold nanostructures were obtained by monitoring the substrate temperature to be higher than room temperature as mentioned in the "experimental details" section. "P" and "I" gold films were formed with the wafer kept at temperatures of 100 and 80 °C, respectively. And the "D" gold film was evaporated while the substrate was cooling down from 80 °C to the room temperature. In detail, after the temperature of the substrate was elevated to 80 °C, we turned off the current in the resistor and then carried out the deposition process.

The morphological changes as the substrate temperature varies can be explained by referring to other related works. In an early report, the authors have demonstrated the considerable effect of substrate temperature on the nucleation and growth of gold films through vapor deposition on single crystal graphite [25]. As the temperature of substrate increases to or above 200 °C, the greater kinetic-controlled island growth results in much more prominent coalescence and grain growth events, so that more three-dimensional and geometrical metal islands can be observed [25]. Based on the same principle, the observed morphologies of gold films on graphene surface here agree well with those shown on graphite surface. Moreover, the "P" gold film, which consists of geometrical gold islands, was realized on single layer graphene at a relatively low substrate temperature of 100 °C (Fig. 1(a)). In our earlier work, thickness-dependent morphologies of

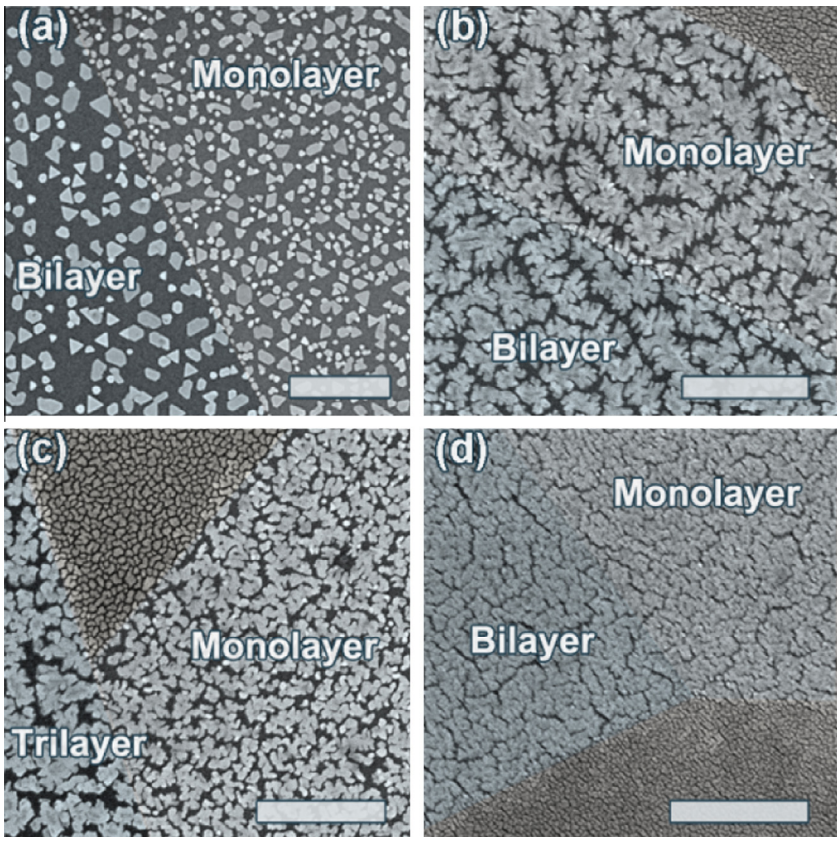

Fig. 1 – Typical SEM images of n-layer graphenes deposited with different Au nanostructures. Scale bar: 500 nm. (a) Polygons. (b) Dendrites. (c) Irregular islands. (d) Dense clusters.

gold thermally deposited onto n-layer graphenes were observed, and the densest gold particles on monolayer graphene was attributed to its highest surface diffusion barrier among n-layer graphenes [24]. In this work, with substrate at higher temperatures during deposition, the shift in the surface free energy or the surface diffusion barrier within graphene is more prominent, so that the morphologies of gold films are expected to change more easily on graphene than on graphite. Studies on the post high temperature annealing of gold films on graphene/graphite surfaces also showed similar

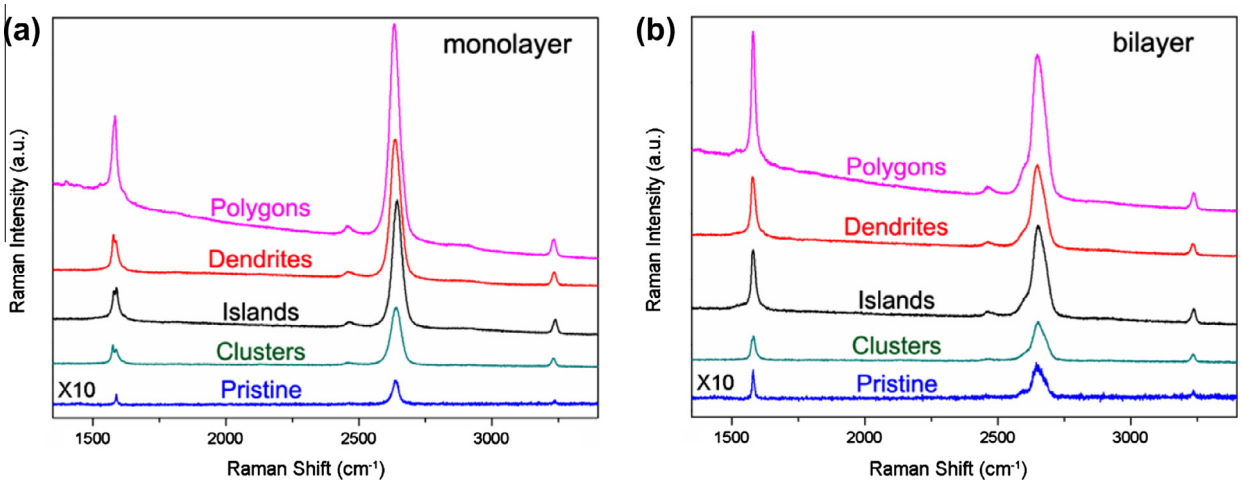

Fig. 2 – The comparison on the Raman spectra of pristine and four different Au nanostructures deposited (a) monolayer and (b) bilayer graphenes at 633 nm laser excitation. The bottom blue curves are the normal Raman spectra, and the other curves are the SERS spectra after Au with four kinds of morphologies was deposited. The normal Raman spectra have been magnified by a factor of 10 to make it clear. (For interpretation of the references to colour in this figure legend, the reader is referred to the web version of this article.)

trend. When heating to 600 °C, the {111} face of Au particles epitaxially grows along the {0001} face of graphite [26]. While on ~700 layer graphene flakes, Luo et al. presented similar gold patterns by annealing at 400 °C after deposition [27]. As for the dendritic gold pattern ("D" gold film), a possible explanation is proposed here as well. Due to the high temperature in the beginning, the nucleation of gold tends to be scattered and the saturated islands have bigger size. Then, as the temperature was decreasing, the atom mobilities were decreasing, thus the following gold nanoparticles would pick a nearby growing island in the coalescence process and form a smaller island during recrystalization. That makes the typical Au pattern where big nuclei appear in the center surrounded by small branches.

3.2. *SERS of graphene*

Fig. 2 displays the representative normal Raman and SERS spectra of monolayer and bilayer graphenes using 633 nm excitation source. Compared with pristine graphene, significant Raman enhancing effects of four different Au nanostructures on the Raman signal of monolayer and bilayer graphenes can be clearly observed. Meanwhile, no obvious defect-related D or D′ peak is observed in the SERS spectra, suggesting the absence of a significant number of defects in gold-deposited graphene.

The enhancement factors of G and 2D bands for n-layer graphenes covered by these four different kinds of gold films are calculated and drawn in Fig. 3. Because the frequency integrated area under each peak is robust with respect to perturbations of the phonon states [28], the EF is determined from the integrated intensity of each band before and after Au deposition. Throughout our measurements, typical 4–6 spectra were acquired on each surface and the spot-to-spot variation is small compared to the overall EF. From the curves presented in Fig. 3, several distinct features can be found. Firstly, the EF decreases with increasing the layer numbers for both G and 2D bands. This phenomenon consists with previous results got by Lee et al., and they attributed the largest EF in monolayer graphene to the strongest interaction between metal and monolayer graphene [20,21]. In addition, we calculated the EF for ~10 layers of graphene (the number "N" in Fig. 3). It can be seen that the EF drops obviously from monolayer to bilayer graphene, and then declines slowly for thicker graphene.

Secondly, the SERS EF is much higher in the G band than that in the 2D band for n-layer graphenes, indicating that G band is more susceptible to SERS than 2D band [20]. The G band is associated with the doubly degenerate zone center E_{2g} phonon mode, and is the only band coming from a normal first order Raman scattering process in graphene. So the peak shape is highly dominated by the phonon dispersion, and can be used to probe any modification to the flat geometrical structure of graphene [29]. On the other hand, the 2D band originates from a second-order, double-resonant (DR) Raman scattering mechanism involving two phonons near the K point, which has a strong dependence on any perturbation to the electronic and/or phonon structure of graphene [30]. Apart from metal-induced SERS effect, the G band also shows more sensitive to the environment than the 2D band in many cases. For example, the G line was found to exhibit strong and symmetric stiffening, while the 2D line only presents weak and slightly asymmetric stiffening for graphene with low electron/hole doping. The width of the 2D line is, in contrast to the G line, almost doping independent [31].

Finally, the comparison result of the enhancement effect among these four gold nanostructures can be concluded as: P > D ≈ I > C. Specifically, the maximum SERS enhancement factors are 272 for G band and 147 for 2D band, which are much higher than the previously reported results [20]. As is known, SERS from metal substrates is mainly due to the coupled SPR absorption and the resulting increased electric field strength at the molecule. Therefore, we would like to interpret this morphology-dependent SERS in terms of EM. The enhanced Raman signal strength of Au nanostructures is dependent upon multiple factors including size, shape, den-

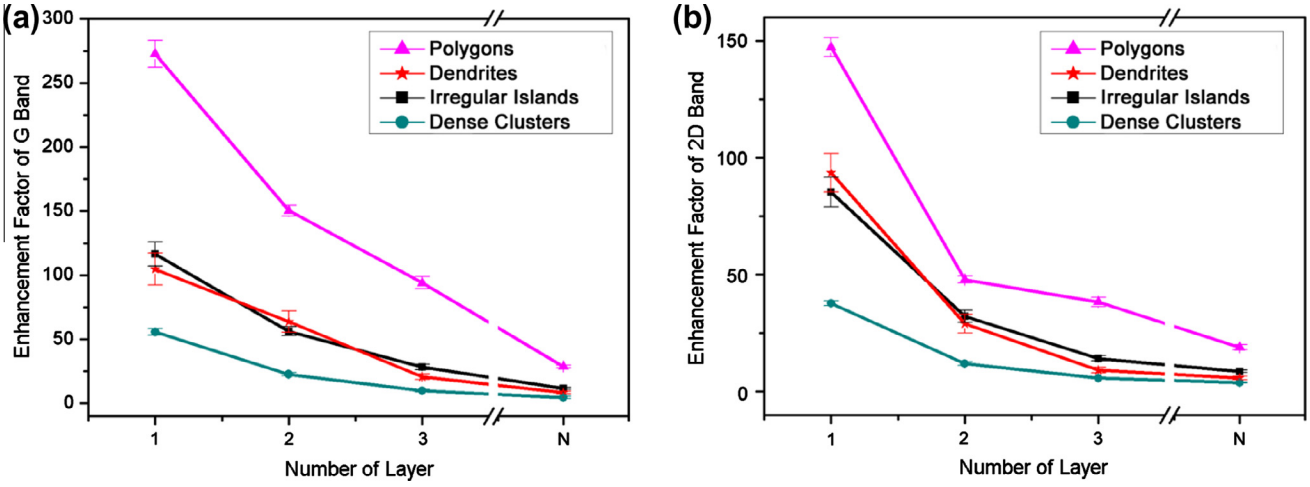

Fig. 3 – Raman enhancement factors of (a) the G band and (b) the 2D band calculated from the integrated intensities of SERS and normal Raman spectra. The lines in different colors and symbols represent the different gold film morphologies as labeled in the right top corners. "N" represents a number around ten.

sity, as well as the orientation and conformation of the tested molecule (i.e. graphene in this case). It has been documented that the optimum radius of Au nanoparticles (or aggregates) for SERS is around 60 nm [32], below which the SERS signal decreases with smaller size. For the "C" gold film, the size is the smallest among these four kinds of gold films (around 30 nm), which may account for its weakest EF. More importantly, the SERS effect is strongly affected by the shape of nanostructures. For metal nanoparticles with sharp features (such as rods or triangles), increased fields can be found near the edges or at the tips of nanoparticles, individually creating much more "hot spots"—areas providing efficient Raman enhancement [33]. Therefore, faceted nanoparticles have an advantage over normal ones for SERS. As discussed above, with the substrate temperature increasing, the Au particles on graphene will coalesce into more three-dimensional and geometrical islands. Moreover, certain edges or facets can be found, as expected, to lie along the crystallographic direction of the underlying graphene. Then the polarizability, to a good approximation, the dipole moments of the uncovered atoms of graphene will lie near the edges and tips of the gold nanostructures (i.e. "hot spots"). Besides, theoretical calculations have provided the distribution of the electric field vectors around a metal triangle, with the orientation perpendicular to the metal surface [34]. Therefore, the dipole moments of graphene can be assumed to be parallel to the electrical field vector of the enhanced light field, leading to strong SERS activity [14]. As a result, we propose that the more faceted gold particles with directional alignment there are, the greater SERS effect will be attained. Consequently, gold films obtained through higher substrate temperature all have larger EFs than the normal "C" gold film. And for the "D" and "P" gold films, although the "D" gold film seems to contain the largest number of facet gold particles, its Raman enhancement effect is less than the "P" gold film. This could be explained as due to the different size, distribution and alignment of the facet gold particles. In the "D" gold film, small facet gold particles are randomly distributed surrounding the middle gold clusters, and their tips are not sharp. In contrast, almost every gold island in the "P" gold film is clearly geometrical with rather big size, and their edges are directional aligned lying along the crystallographic direction of the underlying graphene, which can contribute to large Raman signals as stated earlier. As a result, the "P" gold film can provide a maximum EF.

3.3. *The interaction between gold and graphene*

Fig. 4(a–d) illustrate the results of the deconvolution of the G bands from monolayer graphene in Fig. 2(a). After evaporating 4 nm thick gold, the G bands of monolayer graphenes split into two peaks whereas no obvious splitting is spotted for thicker graphenes. It is noted from early study that the extent of charge transfer between gold and graphene is small [35]. And G band splitting has been spotted as the Raman characteristics of graphene under anisotropic strain [12,36–38]. Thereby, the splitting of G band investigated here should be mainly due to the mechanical interaction between Au and graphene caused by lattice mismatch. As commented previously, G band can probe the variation in the structure of graphene and it is highly sensitive to the strain effect. To be more specific, when the C–C bond lengths and angles of graphene are modified by strain, the hexagonal symmetry of graphene is broken. Thus the G band can split into two sub-

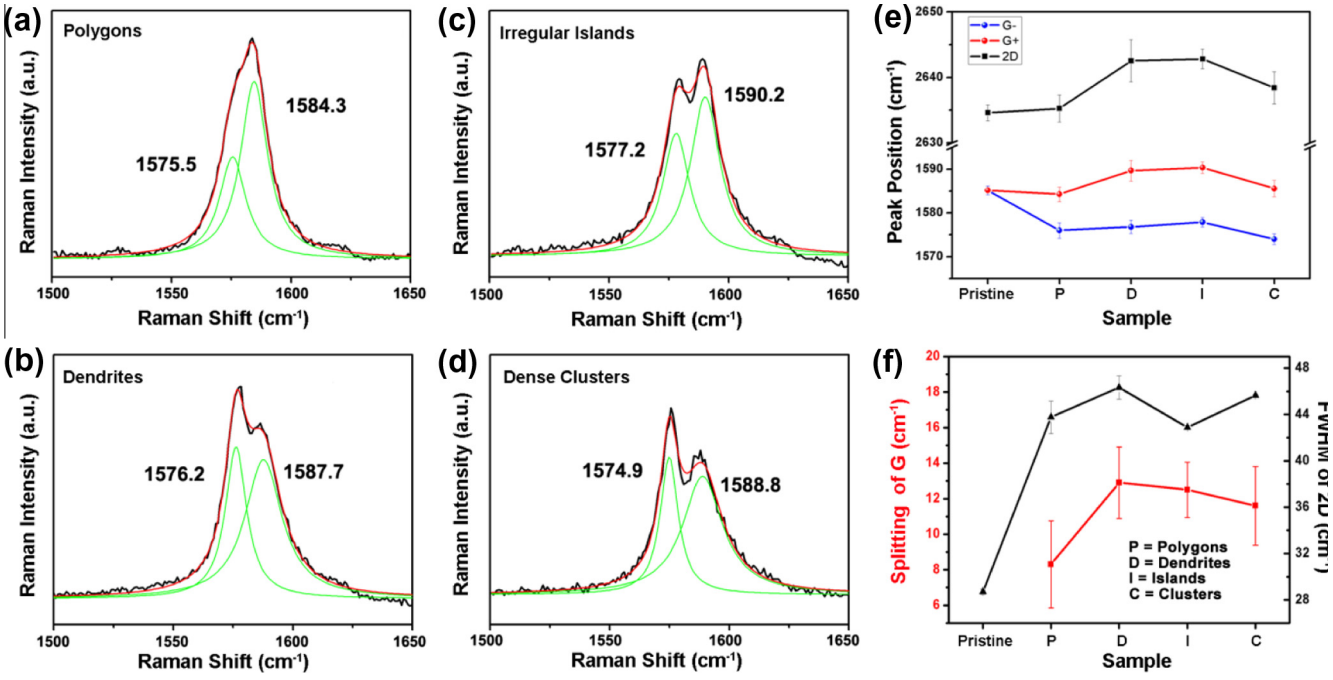

Fig. 4 – (a–d) Deconvolution of the G bands taken from monolayer graphenes with the four Au films: (a) Polygons; (b) dendrites; (c) irregular islands; (d) dense clusters. (e) The frequencies of the fitted G^-, G^+ and 2D peaks. (f) The splitting of the G band and the 2D peak width for different samples.

bands, which are called G^+ and G^- according to their energy, by removing the energy degeneracy of two optical phonons at the Gamma point [10,36].

Typically, all the 2D, G^+ and G^- modes of graphene under uniaxial tensile strain red shift [12,36,37], while compressive strain leads to hardening of these phonons (blue shift) [38]. In this experiment, the G^+ peaks slightly blue shift and the G^- peaks show a ~10 cm^{-1} red shift, while the 2D peaks blue shift with different magnitudes compared to the pristine graphene samples (Fig. 4(e)). The unusual Raman shift behavior here is attributed to a non-systematic and nonuniform strain induced by the thermally deposited gold. In this case, the 2D peak is a more appropriate indicator of the strain state. For example, in the analysis of physisorption strain of graphene on Cu substrate, the G peak was used to probe the carrier density and the strain was explored by the 2D peak [39]. When investigating the effect of mechanical compression on CVD graphene consisting of small domains, Bissett et al. also found that the 2D band upshifts as expected while the G band surprisingly downshifts [40]. These findings can be understood from the different origins of the Raman G and 2D modes. The G band, which is due to a first-order single phonon process, is affected by not only strain but also other factors. On the other hand, the 2D band, which originates from the double resonance processes involving two iTO phonons, is affected mainly by strain within a crystalline domain through the changes in the electronic band structure [40]. Consequently, the blueshift of the 2D band here suggests an overall compressive strain in these gold covered samples. Moreover, we also observe a ~1.5 times larger full-width-at-half-maximum (FWHM) of the 2D peaks as shown in Fig. 4(f). This is consistent with the previous studies of graphene existing inhomogeneous distribution of strain [39]. Additionally, the absence of splitting in the G peaks and shift of the 2D bands for thicker graphenes suggests the weaker force and strain induced by gold. It supports the proposal that the larger EF in monolayer graphene than in thicker graphenes is related to the stronger interaction as discussed in the previous section.

When decreasing ribbon thickness, phonon splitting has been evidenced in VO_x nano-ribbons and is well explained by a new proposed theory model [41]. What is more, the V^{5+}/V^{4+} ratio in the core–shell geometries of the ribbons can be determined from the phonon splitting, indicating rich information provided by Raman spectra of materials in split phonons. Thereby, we now consider the different extents of the G band splitting in the SERS spectra to get more information. They also show dependence on the gold morphologies, which is summarized in Fig. 4(f). The extent of splitting can be listed in a descending order as: 13.0 cm^{-1} for the "D" gold film, 12.5 cm^{-1} for the "I" gold film, 11.6 cm^{-1} for the "C" gold film and 8.3 cm^{-1} for the "P" gold film (i.e. D > I > C > P). Compared to their enhancement effect, it can be found that except "P", a gold film which provides a larger EF will have a larger splitting. Huang et al. [36] and Mohiuddin et al. [37] observed that the splitting of the Raman G mode of graphene will increase with increasing strain. Therefore, we can infer that gold films which apply a larger external force to monolayer graphene will usually give rise to a larger EF. In contrast, the "P" gold film which has the largest EF exhibits the least G band splitting and the least 2D band blueshift. That means the geometrical gold islands can remarkably enhance the Raman cross section of graphene while exerting little strain on graphene. The small strain effect from the "P" gold film may be related to the relatively high temperature during thermal evaporation, which will release the compression in graphene sheet. Another reason is that geometrical gold particles tend to follow along the crystallographic direction of graphene, thus causing less strain from lattice mismatch.

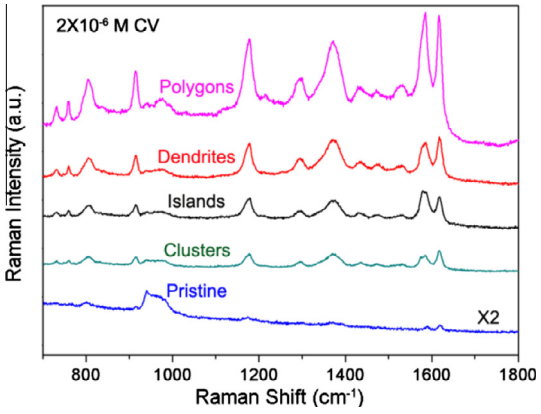

Fig. 5 – Raman spectra of CV molecules deposited on gold-decorated monolayer graphene with 633 nm laser excitation. The concentration of CV solution is 2×10^{-6} M.

3.4. *SERS of crystal violet*

Next, we would like to test the enhancement effects of these gold covered graphenes as SERS substrates. As we have studied previously [23], CV dye molecules, which can provide a relatively rigorous test of the SERS, were deposited by the procedures described in the "experimental details" section. Fig. 5 presents the typical Raman spectra obtained from CV on the four surfaces and on pristine graphene for comparison. The SERS of CV on pristine monolayer graphene has been attributed to the chemical bonding effect in the CV–graphene complex and the signal is relatively weak at 633 nm [23]. On the other hand, 633 nm excitation is close to the SPR wavelength of aggregated Au nanoparticles. The gold assisted Raman enhancement originates from EM, which usually contributes several orders of magnitude more than that based on CM. As a result, systems combined with graphene and gold provide more intense SERS signal here. Furthermore, the enhanced efficiency of CV molecules supported by these gold films exactly follows the same order as that in the SERS of graphene, that is, P > D ≈ I > C. The qualitative agreement between two experimental results nicely illustrates the different SERS effects in the studied Au nanostructures. And it proves that the "P" gold film on graphene can strongly enhance Raman signals of graphene itself as well as other test molecules adsorbed on its surface.

4. Conclusions

The SERS of graphene was investigated by thermally depositing gold films of 4 nm on graphene. By controlling the sub-

strate temperatures, we obtained gold films with four different surface morphologies of polygons, dendrites, irregular islands and dense clusters, which are denoted as P, D, I and C, respectively. The decreasing order of EFs for graphene and CV molecules in these gold films is found to be: P > D ≈ I > C. Furthermore, the G band of gold-covered monolayer graphene splits into two peaks, indicating some mechanical modification of graphene given by the gold deposition. The extent of splitting is also dependent on gold morphologies, which is ordered from high to low as D > I > C > P. The least G peak splitting and the maximum enhancement effect for both graphene and CV are obtained from the "P" gold film, suggesting its potential application in probing fine structural characteristics by SERS. The mechanisms for these observations are discussed qualitatively. The results of this study offer valuable information for the research of both graphene and SERS, also for the understanding of the interaction between metals and graphene.

Acknowledgements

This work is supported by the Singapore National Research Foundation under NRF RF award No. NRF-RF2010-07 and by "973" Program of Ministry of Science and Technology of China (Grant No. 2006CB932402).

Appendix A. Supplementary data

Supplementary data associated with this article can be found, in the online version, at http://dx.doi.org/10.1016/j.carbon.2013.03.043.

REFERENCES

[1] Gupta A, Chen G, Joshi P, Tadigadapa S, Eklund PC. Raman scattering from high-frequency phonons in supported n-graphene layer films. Nano Lett 2006;6(12):2667–73.
[2] Cong CX, Yu T, Saito R, Dresselhaus GF, Dresselhaus MS. Second-order overtone and combination Raman modes of graphene layers in the range of 1690–2150 cm(−1). ACS Nano 2011;5(3):1600–5.
[3] Ni ZH, Liu L, Wang YY, Zheng Z, Li LJ, Yu T, et al. G-band Raman double resonance in twisted bilayer graphene: evidence of band splitting and folding. Phys Rev B 2009;80(12):125404.
[4] Cong C, Yu T, Sato K, Shang J, Saito R, Dresselhaus GF, et al. Raman characterization of ABA- and ABC-stacked trilayer graphene. ACS Nano 2011;5(11):8760–8.
[5] Malard LM, Nilsson J, Elias DC, Brant JC, Plentz F, Alves ES, et al. Probing the electronic structure of bilayer graphene by Raman scattering. Phys Rev B 2007;76(20):201401.
[6] Luo ZQ, Yu T, Ni ZH, Lim SH, Hu HL, Shang JZ, et al. Electronic structures and structural evolution of hydrogenated graphene probed by Raman spectroscopy. J Phys Chem C 2011;115(5):1422–7.
[7] You YM, Ni ZH, Yu T, Shen ZX. Edge chirality determination of graphene by Raman spectroscopy. Appl Phys Lett 2008;93(16):163112.
[8] Gupta AK, Russin TJ, Gutierrez HR, Eklund PC. Probing graphene edges via Raman scattering. ACS Nano 2009;3(1):45–52.
[9] Peimyoo N, Yu T, Shang JZ, Cong CX, Yang HP. Thickness-dependent azobenzene doping in mono- and few-layer graphene. Carbon 2012;50(1):201–8.
[10] Dong XC, Shi YM, Zhao Y, Chen DM, Ye J, Yao YG, et al. Symmetry breaking of graphene monolayers by molecular decoration. Phys Rev Lett 2009;102(13):135501.
[11] Yu T, Ni ZH, Du CL, You YM, Wang YY, Shen ZX. Raman mapping investigation of graphene on transparent flexible substrate: the strain effect. J Phys Chem C 2008;112(33):12602–5.
[12] Ni ZH, Yu T, Lu YH, Wang YY, Feng YP, Shen ZX. Uniaxial strain on graphene: Raman spectroscopy study and band-gap opening. ACS Nano 2008;2(11):2301–5.
[13] Ko H, Singamaneni S, Tsukruk VV. Nanostructured surfaces and assemblies as SERS media. Small 2008;4(10):1576–99.
[14] Zhang JZ, Noguez C. Plasmonic optical properties and applications of metal nanostructures. Plasmonics 2008;3(4):127–50.
[15] Sun YG, Xia YN. Shape-controlled synthesis of gold and silver nanoparticles. Science 2002;298(5601):2176–9.
[16] Arenas JF, Soto J, Tocon IL, Fernandez DJ, Otero JC, Marcos JI. The role of charge-transfer states of the metal–adsorbate complex in surface-enhanced Raman scattering. J Chem Phys 2002;116(16):7207–16.
[17] Wang YY, Ni ZH, Shen ZX, Wang HM, Wu YH. Interference enhancement of Raman signal of graphene. Appl Phys Lett 2008;92(4):043121.
[18] Gao LB, Ren WC, Liu BL, Saito R, Wu ZS, Li SS, et al. Surface and interference coenhanced Raman scattering of graphene. ACS Nano 2009;3(4):933–9.
[19] Schedin F, Lidorikis E, Lombardo A, Kravets VG, Geim AK, Grigorenko AN, et al. Surface-enhanced Raman spectroscopy of graphene. ACS Nano 2010;4(10):5617–26.
[20] Lee J, Shim S, Kim B, Shin HS. Surface-enhanced Raman scattering of single- and few-layer graphene by the deposition of gold nanoparticles. Chem Eur J 2011;17(8):2381–7.
[21] Lee J, Novoselov KS, Shin HS. Interaction between metal and graphene: dependence on the layer number of graphene. ACS Nano 2011;5(1):608–12.
[22] Ferrari AC, Meyer JC, Scardaci V, Casiraghi C, Lazzeri M, Mauri F, et al. Raman spectrum of graphene and graphene layers. Phys Rev Lett 2006;97(18):187401.
[23] Qiu C, Zhou H, Yang H, Chen M, Guo Y, Sun L. Investigation of n-layer graphenes as substrates for Raman enhancement of crystal violet. J Phys Chem C 2011;115(20):10019–25.
[24] Zhou HQ, Qiu CY, Liu Z, Yang HC, Hu LJ, Liu J, et al. Thickness-dependent morphologies of gold on N-layer graphenes. J Am Chem Soc 2010;132(3):944–6.
[25] Wayman CM, Darby TP. Nucleation and growth of gold films on graphite: II. The effect of substrate temperature. J Cryst Growth 1975;28(1):53–67.
[26] Evans EL, Bahl OP, Thomas JM. The decoration of, and epitaxial growth of gold on, graphite surfaces. Carbon 1967;5(6):587–8. IN23-IN24, 9.
[27] Luo ZT, Somers LA, Dan YP, Ly T, Kybert NJ, Mele EJ, et al. Size-selective nanoparticle growth on few-layer graphene films. Nano Lett 2010;10(3):777–81.
[28] Basko DM, Piscanec S, Ferrari AC. Electron–electron interactions and doping dependence of the two-phonon Raman intensity in graphene. Phys Rev B 2009;80(16):165413.
[29] Dresselhaus MS, Jorio A, Hofmann M, Dresselhaus G, Saito R. Perspectives on carbon nanotubes and graphene Raman spectroscopy. Nano Lett 2010;10(3):751–8.
[30] Malard LM, Pimenta MA, Dresselhaus G, Dresselhaus MS. Raman spectroscopy in graphene. Phys Rep 2009;473(5–6):51–87.

[31] Stampfer C, Molitor F, Graf D, Ensslin K, Jungen A, Hierold C, et al. Raman imaging of doping domains in graphene on SiO_2. Appl Phys Lett 2007;91(24):243901.
[32] Krug JT, Wang GD, Emory SR, Nie S. Efficient Raman enhancement and intermittent light emission observed in single gold nanocrystals. J Am Chem Soc 1999;121(39):9208–14.
[33] Esenturk EN, Walker ARH. Surface-enhanced Raman scattering spectroscopy via gold nanostars. J Raman Spectrosc 2009;40(1):86–91.
[34] Jackel F, Kinkhabwala AA, Moerner WE. Gold bowtie nanoantennas for surface-enhanced Raman scattering under controlled electrochemical potential. Chem Phys Lett 2007;446(4–6):339–43.
[35] Subrahmanyam KS, Manna AK, Pati SK, Rao CNR. A study of graphene decorated with metal nanoparticles. Chem Phys Lett 2010;497(1–3):70–5.
[36] Huang MY, Yan HG, Chen CY, Song DH, Heinz TF, Hone J. Phonon softening and crystallographic orientation of strained graphene studied by Raman spectroscopy. Proc Natl Acad Sci 2009;106(18):7304–8.
[37] Mohiuddin TMG, Lombardo A, Nair RR, Bonetti A, Savini G, Jalil R, et al. Uniaxial strain in graphene by Raman spectroscopy: G peak splitting, Grüneisen parameters, and sample orientation. Phys Rev B 2009;79(20):205433.
[38] Ni ZH, Chen W, Fan XF, Kuo JL, Yu T, Wee ATS, et al. Raman spectroscopy of epitaxial graphene on a SiC substrate. Phys Rev B 2008;77(11):115416.
[39] He R, Zhao L, Petrone N, Kim KS, Roth M, Hone J, et al. Large physisorption strain in chemical vapor deposition of graphene on copper substrates. Nano Lett 2012;12(5):2408–13.
[40] Bissett MA, Izumida W, Saito R, Ago H. Effect of domain boundaries on the Raman spectra of mechanically strained graphene. ACS Nano 2012;6(11):10229–38.
[41] Mwakikunga BW, Maaza M, Hillie KT, Arendse CJ, Malwela T, Sideras-Haddad E. From phonon confinement to phonon splitting in flat single nanostructures: a case of VO_2@V_2O_5 core–shell nano-ribbons. Vib Spectrosc 2012;61:105–11.